The relationship between toluene content of the solutions (1T7I, 1T5I, 1T3I) and D_c value was plotted and is shown in Fig. 4, where the D_c value increases linearly with increasing content of toluene. This fact implies that the D_c value depends on the supersaturation of C_{60}.

The linear curve fit is expressed as $D_c = 13.5x + 83$ (nm), where x is the concentration of toluene in the C_{60}–toluene–IPA solution. Although the fitted curve does not possess the rigorous quantitative accuracy due to the above hypothetically set D_c values, it is qualitatively suggested that the D_c value increases with decrease in supersaturation caused by the intermixing of toluene and IPA. If the above fitted curve is assumed to hold for the concentration of 100% toluene, the D_c value in the solution without IPA will become 1432 nm. This diameter of 1432 nm may be regarded as the critical diameter of C_{60} needle-like crystals that can be grown in a C_{60}-saturated toluene solution at 20 °C. The D_c value approaches 83 nm with decreasing the toluene concentration, which suggests that the diameter of C_{60}NWs can be smaller than 100 nm as described in the introductory section. Hence the optimization of solvent ratio is a crucial factor for the controlled growth of C_{60}NWs.

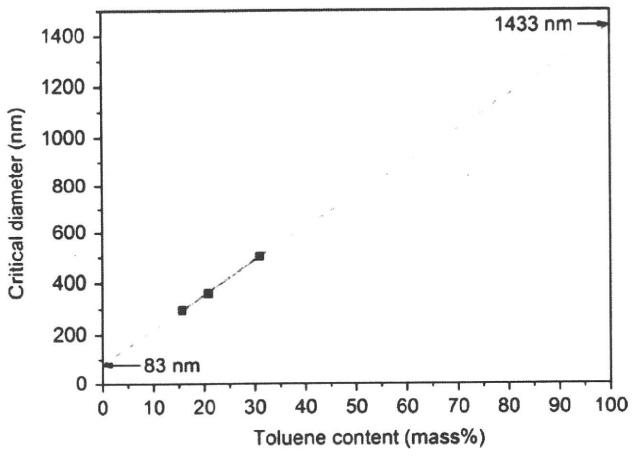

Fig. 4. Critical diameter (D_c) of C_{60}NWs plotted as a function of toluene content (mass %) in the C_{60}–toluene–IPA solutions.

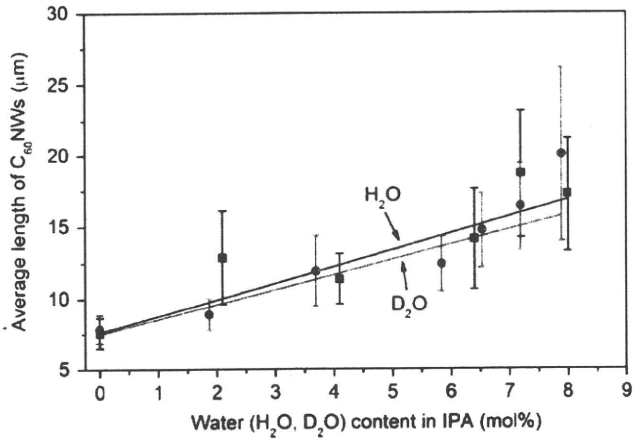

Fig. 5. Average length of C_{60}NWs plotted as a function of water (H_2O, D_2O) content in IPA for the growth period of 24 h at 20 °C.

3.2. Effect of water on the growth of C_{60}NWs

In our preliminary experiment, the addition of water was observed to promote growth of C_{60}NWs [36]. In order to confirm this effect of water, experiments have been performed by use of D_2O as well as H_2O and the result of length measurement of C_{60}NWs is shown in Fig. 5 for cases of both H_2O and D_2O additions.

The horizontal axis is expressed in mole percentage to compare the effect of water by the number of added water molecules. Since the addition of excess amount of water was shown to result in destabilization of C_{60}NWs by our previous experiment [36], the water content in solutions was set to be small. The length value for each data point is the mean value of

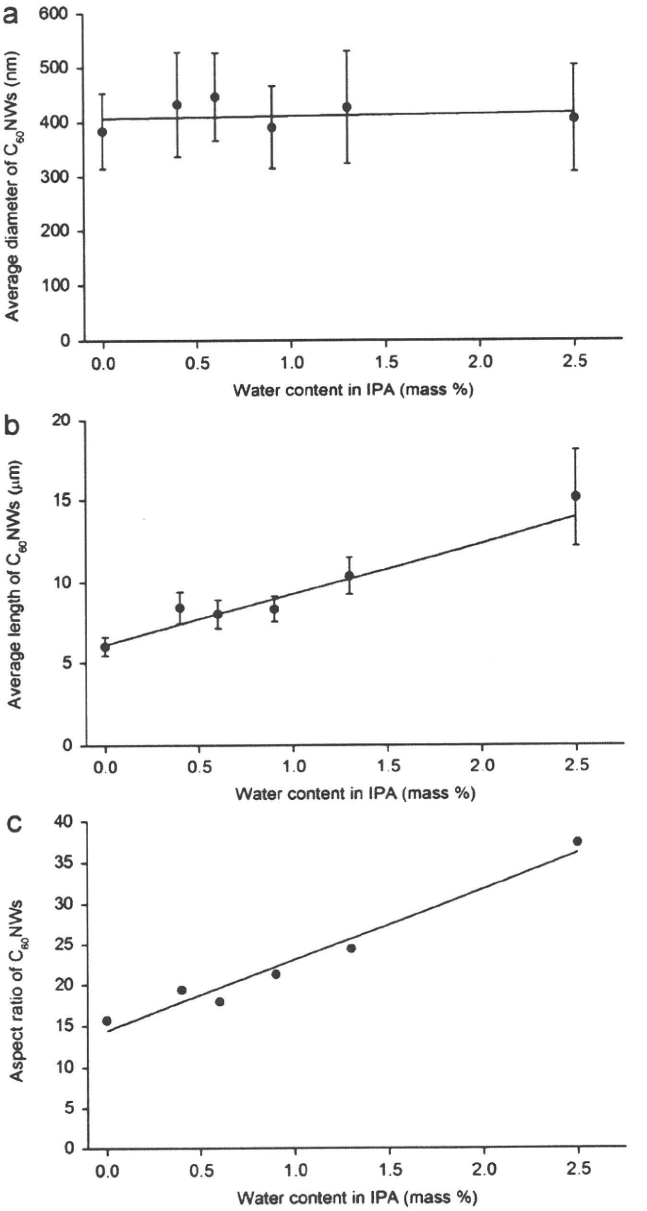

Fig. 6. (a) Average diameter, (b) average length and (c) aspect ratio of the C_{60}NWs plotted as a function of water content (mass %) in IPA. C_{60}NWs were grown at 20 °C for 24 h.

exactly 100 C_{60}NWs. It is clearly shown that the addition of small amount of H_2O and D_2O promotes growth of C_{60}NWs.

The positive effect of H_2O on growth of C_{60}NWs is confirmed by the experiment of D_2O addition, which can eliminate the effect of impurity H_2O contained in the used toluene and IPA reagents. Although the addition of D_2O promotes growth of C_{60}NWs, the effect of D_2O is shown to be a little weaker than the effect of H_2O addition. The small discrepancy between the two linear curves is considered to be caused by a deuterium isotope effect.

Although length of the C_{60}NWs increases with increasing content of water in the solution, diameter of the C_{60}NWs remains almost constant as shown in Fig. 6(a). Fig. 6(b) shows the average length of C_{60}NWs plotted as a function of water (H_2O) content for the same sample of C_{60}NWs of Fig. 6(a), where the whisker length is shown to increase with increasing water content as shown above. The aspect ratio (length/diameter) can be calculated using the data of Fig. 6(a) and 6(b), and is plotted as Fig.6(c). It is found that the aspect ratio can be widely varied between 10 and 40 just

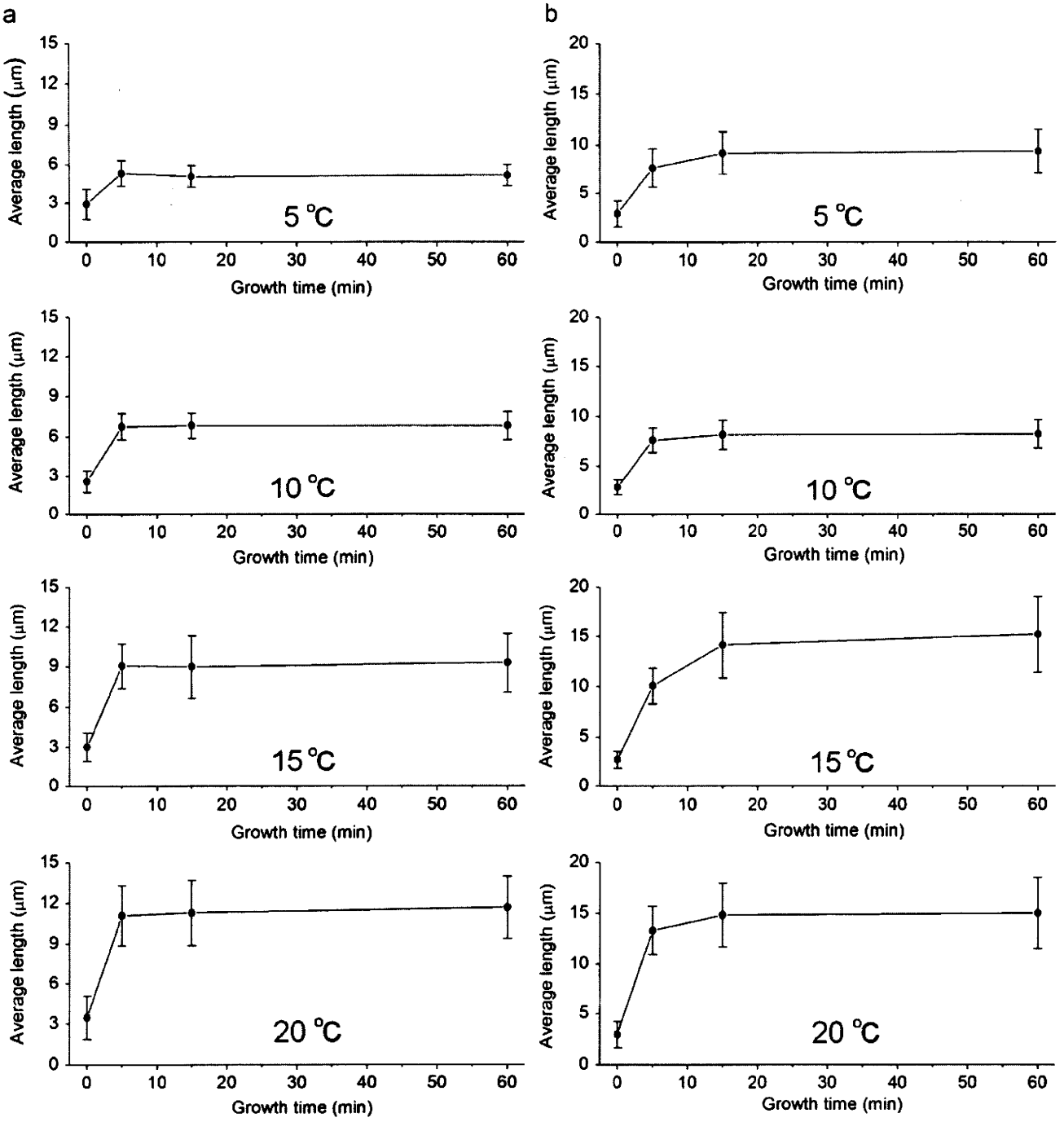

Fig. 7. Average lengths of the C_{60}NWs synthesized by use of IPA containing (a) 1.3 mass % H_2O and (b) 2.5 mass % H_2O, measured as a function of growth time at temperatures between 5 and 20 °C.

by controlling the small content of water. This fact shows that the control of water content in solvents is very important for the length control of C_{60}NWs.

Length of the C_{60}NWs was measured as a function of growth time at temperatures between 5 and 20 °C for each water content in IPA as shown in Fig. 7. Growth time was defined as the elapsed time from the end of the manual mixing. Hence, the C_{60}NWs show finite lengths of a few micrometers at the initial growth time of 0 min in each figure. The growth of C_{60}NWs becomes slower for longer growth time. This phenomenon shows that supersaturation of C_{60} becomes smaller with the growth of C_{60}NWs that consume the dissolved C_{60} molecules.

Measured length growth rates were plotted and are shown in the Arrhenius plots of Figs. 8(a) and (b) as a function of $1/T$, where T is the absolute temperature (K). The length growth rates were calculated from the length increment of the initial 5 min as previously reported [15].

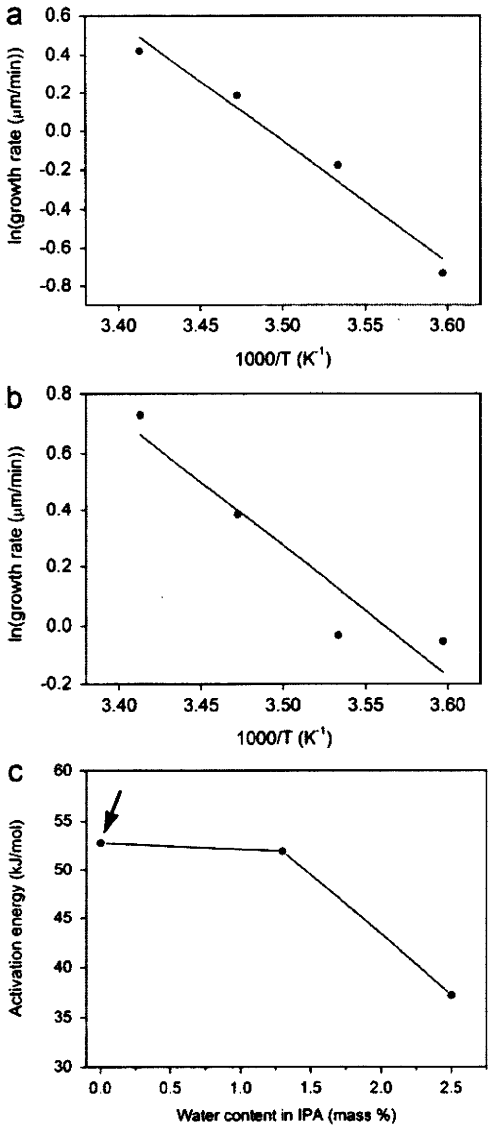

Fig. 8. Arrhenius plots of the length growth rate of C_{60}NWs prepared by use of IPA containing (a) 1.3 mass % H_2O, and (b) 2.5 mass % H_2O and (c) activation energy for the growth of C_{60}NWs plotted as a function of H_2O content in IPA. The data point of 0 mass % H_2O is the value previously reported [15].

The whisker growth activation energy can be calculated from the slope of the Arrhenius plots and is shown as Fig. 8(c). The point marked by arrow is the activation energy of 52.8 kJ/mol measured in our previous experiment using the solvents without water addition [15]. The growth activation energy is found to become smaller with increasing water content. Hence, it is suggested that water acts as a catalyst in the growth of C_{60}NWs.

4. Conclusions

The above results can be summarized as follows:

(1) Morphology of C_{60} precipitates synthesized by the modified LLIP method is strongly influenced by volume ratio of the C_{60}-saturated toluene solution to IPA. The sample prepared using the solution with a volume ratio of 1:1 for toluene and IPA showed the best growth of C_{60}NWs.
(2) C_{60}NWs can grow longer above a critical diameter D_c. D_c value decreases with increasing IPA content in the C_{60}–toluene–IPA solutions.
(3) Length growth of C_{60}NWs is promoted by the addition of small amounts of H_2O, while their diameter remains almost constant. This fact can be utilized to control the aspect ratio of C_{60}NWs.
(4) Positive effect of water addition on growth of C_{60}NWs was also confirmed by the use of D_2O.
(5) Growth activation energy of C_{60}NWs decreased with increasing water content. It is suggested that water catalyzes the growth of C_{60}NWs.

Acknowledgement

The authors are grateful to Dr. Takatsugu Wakahara (NIMS) for his valuable comments and discussions. Part of this research was supported by Health and Labour Sciences Research Grants (H21—Chemistry—Ippan-008) from the Ministry of Health, Labour and Welfare of Japan.

References

[1] K. Miyazawa, J. Nanosci. Nanotechnol. 9 (2009) 41.
[2] K. Miyazawa, A. Obayashi, M. Kuwabara, J. Am. Ceram. Soc. 84 (2001) 3037.
[3] K. Miyazawa, Y. Kuwasaki, A. Obayashi, M. Kuwabara, J. Mater. Res. 17 (2002) 83.
[4] K. Miyazawa, T. Mashino, T. Suga, J. Mater. Res. 18 (2003) 273.
[5] T. Tsuchiya, R. Kumashiro, K. Tanigaki, Y. Matsunaga, M.O. Ishitsuka, T. Wakahara, Y. Maeda, Y. Takano, M. Aoyagi, T. Akasaka, M.T.H. Liu, T. Kato, K. Suenaga, J.S. Jeong, S. Iijima, F. Kimura, T. Kimura, S. Nagase, J. Am. Chem. Soc. 130 (2008) 450.
[6] K. Miyazawa, J. Minato, T. Yoshii, M. Fujino, T. Suga, J. Mater. Res. 20 (2005) 688.
[7] J. Minato, K. Miyazawa, T. Suga, Sci. Technol. Adv. Mater. 6 (2005) 272.
[8] K. Rauwerdink, J.-F. Liu, J. Kintigh, G.P. Miller, Microsc. Res. Tech. 70 (2007) 513.
[9] K. Miyazawa, M. Kuwabara, United States Patent No. US 6890505 B2 2005.
[10] K. Miyazawa, J. Minato, T. Suga, in: Proceedings of the Fourth International Conference on Materials Processing for Properties and Performance (MP3-IV), vol. 4, Tsukuba, Japan, 2005, pp. 291–293.
[11] K. Miyazawa, J.Minato, T. Mashino, T. Yoshii, T. Kizuka, R. Kato, M.Tachibana, T. Suga, in: Proceedings of the Second JSME/ASME International Conference on Materials and Processing 2005—the 13th JSME Materials and Processing Conference (M&P2005), Seattle, USA, 2005, p. SMS-23.
[12] J. Minato, K. Miyazawa, J. Mater. Res. 21 (2006) 529.
[13] K. Miyazawa, C. Ringor, Mater. Lett. 62 (2008) 410.
[14] Y. Zhang, W. Liu, L. Jiang, L. Fan, C. Wang, W. Hu, H. Zhong, Y. Li, S. Yang, J. Mater. Chem. 20 (2010) 953.
[15] K. Hotta, K. Miyazawa, Nano 3 (2008) 355.
[16] Y. Jin, R.J. Curry, J. Sloan, R.A. Hatton, L.C. Chong, N. Blanchard, V. Stolojan, H.W. Kroto, S.R.P. Silva, J. Mater. Chem. 16 (2006) 3715.
[17] S.I. Cha, K. Miyazawa, J.-D. Kim, Chem. Mater. 20 (2008) 1667.
[18] S.I. Cha, D.Y. Lee, K. Miyazawa, T. Wakahara, J. Phys.: Conf. Ser. 159 (2009) 012011.

[19] M. Sathish, K. Miyazawa, J.P. Hill, K. Ariga, J. Am. Chem. Soc. 131 (2009) 6372.
[20] M. Sathish, K. Miyazawa, J. Am. Chem. Soc. 129 (2007) 13816.
[21] A. Masuhara, Z. Tan, H. Kasai, H. Nakanishi, H. Oikawa, Jpn. J. Appl. Phys. 48 (2009) 050206.
[22] M.P. Larsson, J. Kjelstrup-Hansen, S. Lucyszyn, ECS Trans. 2 (2007) 27.
[23] M. Xu, Y. Pathak, D. Fujita, C. Ringor, K. Miyazawa, Nanotechnology 19 (2008) 075712.
[24] K. Ogawa, T. Kato, A. Ikegami, H. Tsuji, N. Aoki, Y. Ochiai, J.P. Bird, Appl. Phys. Lett. 88 (2009) 112109.
[25] M. Sathish, K. Miyazawa, T. Sasaki, Chem. Mater. 19 (2007) 2398.
[26] M. Sathish, K. Miyazawa, T. Sasaki, J. Solid State Electrochem. 12 (2008) 835.
[27] M. Sathish, K. Miyazawa, T. Sasaki, Diamond Relat. Mater. 17 (2008) 571.
[28] M. Sathish, K. Miyazawa, Nano 3 (2008) 409.
[29] K. Miyazawa, J. Minato, H. Zhou, T. Taguchi, I. Honma, T. Suga, J. Eur. Ceram. Soc. 26 (2006) 429.
[30] Q. Wang, Y. Zhang, K. Miyazawa, R. Kato, K. Hotta, T. Wakahara, J. Phys.: Conf. Ser.s 159 (2009) 012023.
[31] P.R. Somani, S.P. Somani, M. Umeno, Appl. Phys. Lett. 91 (2007) 173503.
[32] L.C. Chong, J. Sloan, G. Wagner, S.R.P. Silva, R.J. Curry, J. Mater. Chem. 18 (2008) 3319.
[33] K. Miyazawa, NIMS Now 1 (2003) 2.
[34] M. Tachibana, K. Kobayashi, T. Uchida, K. Kojima, M. Tanimura, K. Miyazawa, Chem. Phys. Lett. 374 (2003) 279.
[35] K. Kobayashi, M. Tachibana, K. Kojima, J. Cryst. Growth 274 (2005) 617.
[36] K. Hotta, K. Miazawa, J. Phys.: Conf. Ser. 159 (2009) 012021.
[37] A.S. Haja Hameed, G. Ravi, R. Jayavel, P. Ramasamy, J. Cryst. Growth 250 (2003) 126.

J Nanopart Res
DOI 10.1007/s11051-010-0132-y

RESEARCH PAPER

The effect of water on the stability of C_{60} fullerene nanowhiskers

Kun'ichi Miyazawa · Kayoko Hotta

Received: 26 July 2010 / Accepted: 26 October 2010

Abstract The morphology of C_{60} precipitates synthesized by using isopropyl alcohol (IPA) added with water was investigated in order to know the effect of water on the growth of C_{60} nanowhiskers (C_{60}NWs) in C_{60}–toluene–IPA solution systems. The stability of C_{60}NWs decreased and granular crystals of C_{60} were formed in the solutions when IPA added with an excess amount of water was used in the liquid–liquid interfacial precipitation method. The C_{60}NWs were found to be destabilized with time in the solutions added with water. The C_{60}NWs dried in air showed similar Raman profiles irrespective of the use of IPA with and without water addition. The Raman profiles of granular C_{60} single crystals showed the base lines much flatter than those of C_{60}NWs, indicating that C_{60}NWs possess a disordered crystal structure. By optimizing the growth condition, short C_{60}NWs with aspect ratios ranging from 3 to 10 and an average length of about 1.8 μm were successfully fabricated. The short C_{60}NWs are expected to be applicable for electrodes of organic thick film solar cells.

K. Miyazawa (✉) · K. Hotta
Fullerene Engineering Group, Exploratory Nanotechnology Research Laboratory, National Institute for Materials Science, 1-1, Namiki Tsukuba, Ibaraki 305-0044, Japan
e-mail: miyazawa.kunichi@nims.go.jp

Published online: 18 November 2010

Keywords Fullerene nanowhisker · Liquid–liquid interfacial precipitation method · LLIP method · C_{60} nanowhisker · Fullerene

Introduction

Since the discovery of C_{60} fullerene nanowhiskers (C_{60}NWs) in 2001 (Miyazawa et al. 2001; Miyazawa 2009), C_{60}NWs have been variously applied for field-effect transistors (FETs) (Ogawa et al. 2006, 2008), fuel cells (Wang et al. 2009), solar cells (Somani et al. 2007), catalysts (Sathish et al. 2008), templates for chemical synthesis (Minato and Miyazawa 2006), and so forth.

C_{60}NWs can be synthesized by the liquid–liquid interfacial precipitation method (LLIP method), where a poor solvent of C_{60} is placed on a C_{60}-saturated good solvent solution (Miyazawa et al. 2002) in order to form a liquid–liquid interface between the C_{60}-saturated good solvent solution and the poor solvent. C_{60} embryo crystals nucleate at the liquid–liquid interface due to the formation of supersaturated C_{60} solution that is caused by the interdiffusion between the good solvent solution and the poor solvent, and grow into long C_{60}NWs. The above LLIP method proposed in 2002 is called the "static LLIP method" which does not accompany such disturbances as caused by ultrasonication,

manual mixing, and so forth. Variously modified LLIP methods that utilize the mixing of good solvent solutions of fullerenes and poor solvents of fullerenes have been developed until today. It has been known that the growth of C_{60}NWs is influenced by light (Tachibana et al. 2003), temperature (Hotta and Miyazawa 2008), solvent ratio, and impurity water (Miyazawa and Hotta 2010). Although the impurity water contained in the solution markedly influences the growth rate of C_{60}NWs, the addition of excess amount of water was found to destabilize the growth of C_{60}NWs in our preliminary experiment (Hotta and Miyazawa 2009).

Hence, in this paper, the influence of water on the morphology of C_{60} precipitates is minutely investigated using D_2O as well as H_2O and it will be shown that the addition of excess amount of water hinders the formation of C_{60}NWs.

On the other hand, C_{60}NWs can grow from several micrometers to the order of millimeters or more in length (Miyazawa and Ringor 2008; Hotta and Miyazawa 2009). Although long C_{60}NWs are suitable for the preparation of non-woven C_{60} sheets (Miyazawa 2003), the size control of short C_{60}NWs is also important in their application. For example, short C_{60}NWs with lengths of several micrometers were successfully applied for the fabrication of organic thick film solar cells (Somani et al. 2007). Recently we showed the synthesis of short C_{60}NWs with lengths less than 5 μm by a modified LLIP method (Miyazawa and Hotta 2010) and have improved the method in order to synthesize much shorter C_{60}NWs with uniform lengths and diameters by optimizing the synthetic condition. Hence, the study to fabricate the short C_{60}NWs will also be presented in this paper.

Experiment

In the synthesis of C_{60}NWs by the LLIP method using solutions containing water, isopropyl alcohol (IPA) (as-received, Wako Pure Chemical Industries, Ltd., Japan) mixed with distilled water (Wako) was gently added to C_{60}-saturated toluene solutions in 10 mL transparent glass bottles at 20 °C. Next, the bottles were capped and manually shaken 30 times and stored in an incubator (SANYO MIR-153) at 20 °C. This modified LLIP method combined with the hand shaking process is named "hand shaking LLIP method", here. The volume ratio of the C_{60}-saturated toluene solutions to IPA containing water was fixed to be 1:1 and the content of water in IPA was set to be less than 4 mass% H_2O. Instead of H_2O, heavy water (D_2O, ISOTEC, 99.96 at%) was also used in order to reduce the effect of impurity H_2O contained in the as-received solvents IPA and toluene and to confirm the experimental reproducibility. The H_2O content of as-received IPA was measured to be 0.02% and that of as-received toluene (Wako) was measured to be 0.01% by a Karl Fischer titrator (Coulometer 831 KF). IPA and toluene were used without further purification. In this paper, "water" normally means H_2O as long as no special notice is indicated. Raman spectroscopy analyses (JASCO NRS-3100, Japan, laser excitation wavelength of 532 nm) were conducted for the C_{60}NWs in order to examine the effect of water addition on the structure of C_{60}NWs.

In preparing short C_{60}NWs, 2.25 mL of toluene solution saturated with C_{60} was poured into a glass bottle (10 mL) and 6.75 mL of IPA was gently added into the bottle to form a liquid–liquid interface at 15 °C, where the solvent volume ratio is 1 (toluene):3 (IPA). Next, the glass bottle was capped and manually shaken 30 times in order to obtain homogeneous embryo crystals and kept in an incubator at a growth temperature of 15 °C for 1 day.

Results and discussion

Morphology change of C_{60} precipitates by addition of water

Figures 1, 2, 3, and 4 show optical microscopy images of the C_{60} precipitates that were formed by using IPA containing different amounts of water (H_2O, D_2O). Figure 1 shows the C_{60} precipitates observed 1 day after the start of synthesis, while Fig. 2 shows those observed 7 days after the start of synthesis for different H_2O contents. Granular C_{60} precipitates appeared for the H_2O contents greater than 2.3 mass% in IPA in the samples of 1 day aging, while in the case of 7 days aging, the granular C_{60} precipitates appeared at a H_2O content of 2.0 mass% in IPA which was lower than the corresponding value of 2.3 mass% H_2O for 1 day aging. The above observation shows that the stability of C_{60}NWs in solution decreases with increasing the H_2O content

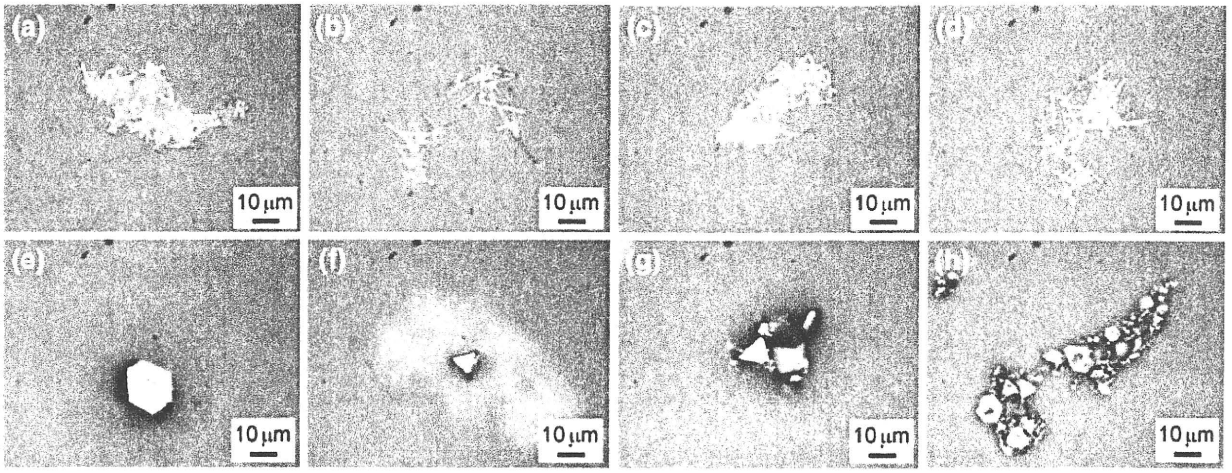

Fig. 1 Optical micrographs of the C_{60} precipitates formed by using IPA with different H_2O contents and aged for 1 day in solutions. **a** 0 mass% H_2O, **b** 0.6 mass% H_2O, **c** 1.3 mass% H_2O, **d** 2.0 mass% H_2O, **e** 2.3 mass% H_2O, **f** 2.5 mass% H_2O, **g** 2.8 mass% H_2O, and **h** 3.8 mass% H_2O

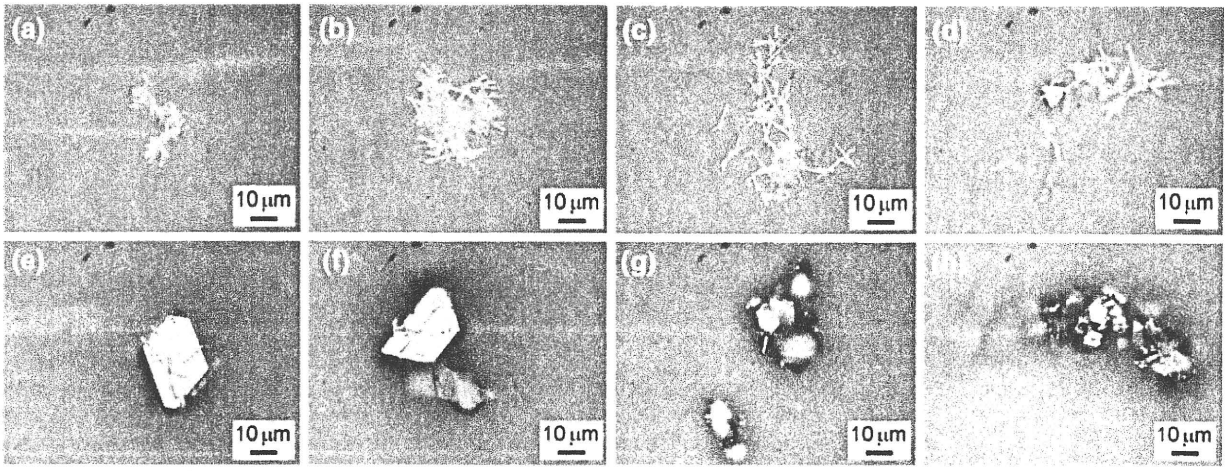

Fig. 2 Optical micrographs of the C_{60} precipitates formed by using IPA with different H_2O contents and aged for 7 days in solutions. **a** 0 mass% H_2O, **b** 0.6 mass% H_2O, **c** 1.3 mass% H_2O, **d** 2.0 mass% H_2O, **e** 2.3 mass% H_2O, **f** 2.5 mass% H_2O, **g** 2.8 mass% H_2O, and **f** 3.8 mass% H_2O

and with time. This experiment by use of the hand shaking LLIP method was repeated once again, and the same results as observed in Fig. 1 were obtained. This good reproducibility of the hand shaking LLIP method was also shown in our previous growth study of C_{60}NWs (Miyazawa and Hotta 2010).

Figure 3 shows the similar observations that were performed using D_2O instead of H_2O. The granular C_{60} crystals appeared for the D_2O contents greater than 2.8 mass% for 1 day aging, while in the case of 7 days aging (Fig. 4), the granular C_{60} crystals appeared at the D_2O contents greater than 1.3 mass% in IPA. Hence, in the case of D_2O addition also, the stability of C_{60}NWs in solution is found to decrease with increasing the amount of added D_2O and with time. Since the experiment using D_2O can reduce relatively the effect of impurity H_2O contained in solution, this observation using D_2O also confirms that the water destabilizes C_{60}NWs in solution. Further it is conjectured that the water would destabilize C_{60}NWs in air for a long time. The above observations suggest that the destabilization of C_{60}NWs occurs in the solutions containing water with concentrations greater than a critical value.

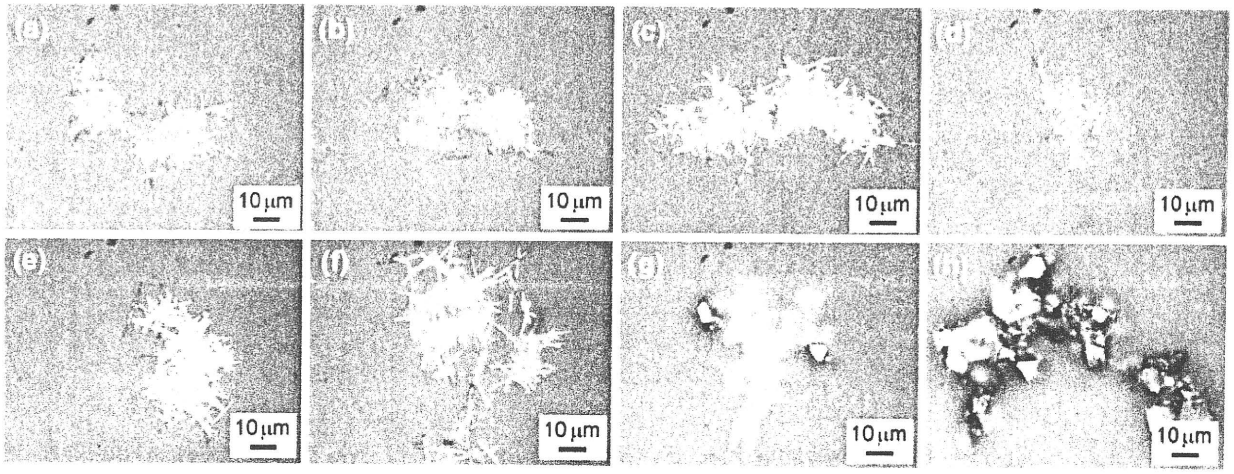

Fig. 3 Optical micrographs of the C_{60} precipitates formed by using IPA with different D_2O contents and aged for 1 day in solutions. **a** 0 mass% D_2O, **b** 0.6 mass% D_2O, **c** 1.3 mass% D_2O, **d** 2.0 mass% D_2O, **e** 2.3 mass% D_2O, **f** 2.5 mass% D_2O, **g** 2.8 mass% D_2O, and **h** 3.8 mass% D_2O

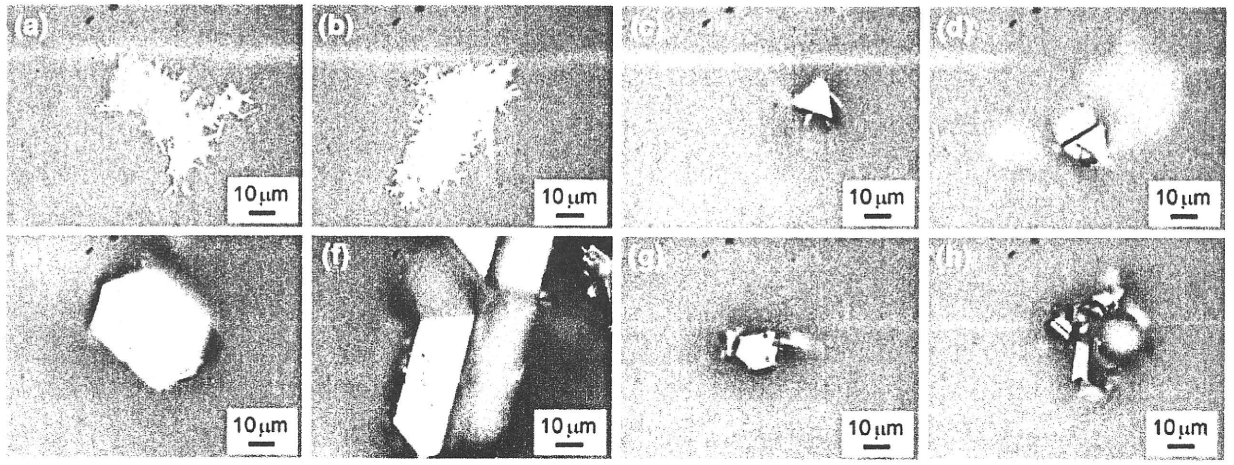

Fig. 4 Optical micrographs of the C_{60} precipitates formed by using IPA with different D_2O contents and aged for 7 days in solutions. **a** 0 mass% D_2O, **b** 0.6 mass% D_2O, **c** 1.3 mass% D_2O, **d** 2.0 mass% D_2O, **e** 2.3 mass% D_2O, **f** 2.5 mass% D_2O, **g** 2.8 mass% D_2O, and **h** 3.8 mass% D_2O

The water molecules have a large dipole moment of 1.85 D (Kemp and Gordon 2008), while IPA molecules have a dipole moment of 1.6 D (Nakao et al. 1997). It is known that the addition of small amounts of water to IPA promotes the growth of C_{60}NWs by lowering the growth activation energy of C_{60}NWs (Miyazawa and Hotta 2010). This fact implies that a high desolvation energy of C_{60} can be lowered by the catalytic effect of water (Hotta and Miyazawa 2008). It is assumed that water molecules reduce the interaction forces between C_{60} molecules and toluene molecules in solution and that the accumulation process of C_{60} molecules on the surface of C_{60}NWs is enhanced. On the other hand, the water molecules are expected to interact strongly with IPA molecules and to form the complicated water–IPA molecular clusters that hinder the interdiffusion between toluene and IPA as reported in a system of water–methyl alcohol (Guo et al. 2003). As a result, the supersaturation degree of C_{60}, the driving force of whisker formation, will be decreased by addition of water and lead to the formation of granular crystals. Actually, we showed that the reduction of supersaturation leads to the formation of granular crystals instead of C_{60}NWs (Miyazawa and Hotta 2010).

Although the reduction of growth activation energy by addition of water enhances the growth

of C_{60}NWs, it is also expected to accelerate the reverse redissolution reaction of C_{60}NWs which leads to the reprecipitation of granular C_{60} crystals. Hence, the formation of granular C_{60} precipitates by addition of excess amounts of water is conjectured to be induced by combination of the following two mechanisms.

(1) Reduction of the supersaturation of C_{60} with time which leads to the nucleation of granular crystals.

(2) Acceleration of the reverse redissolution reaction of C_{60}NWs by the reduction of growth activation energy, leading to the reprecipitation of granular C_{60} crystals.

Raman spectroscopy of the C_{60}NWs synthesized by using IPA added with water

As shown above, the morphology of C_{60} precipitates depends on the content of water added to IPA.

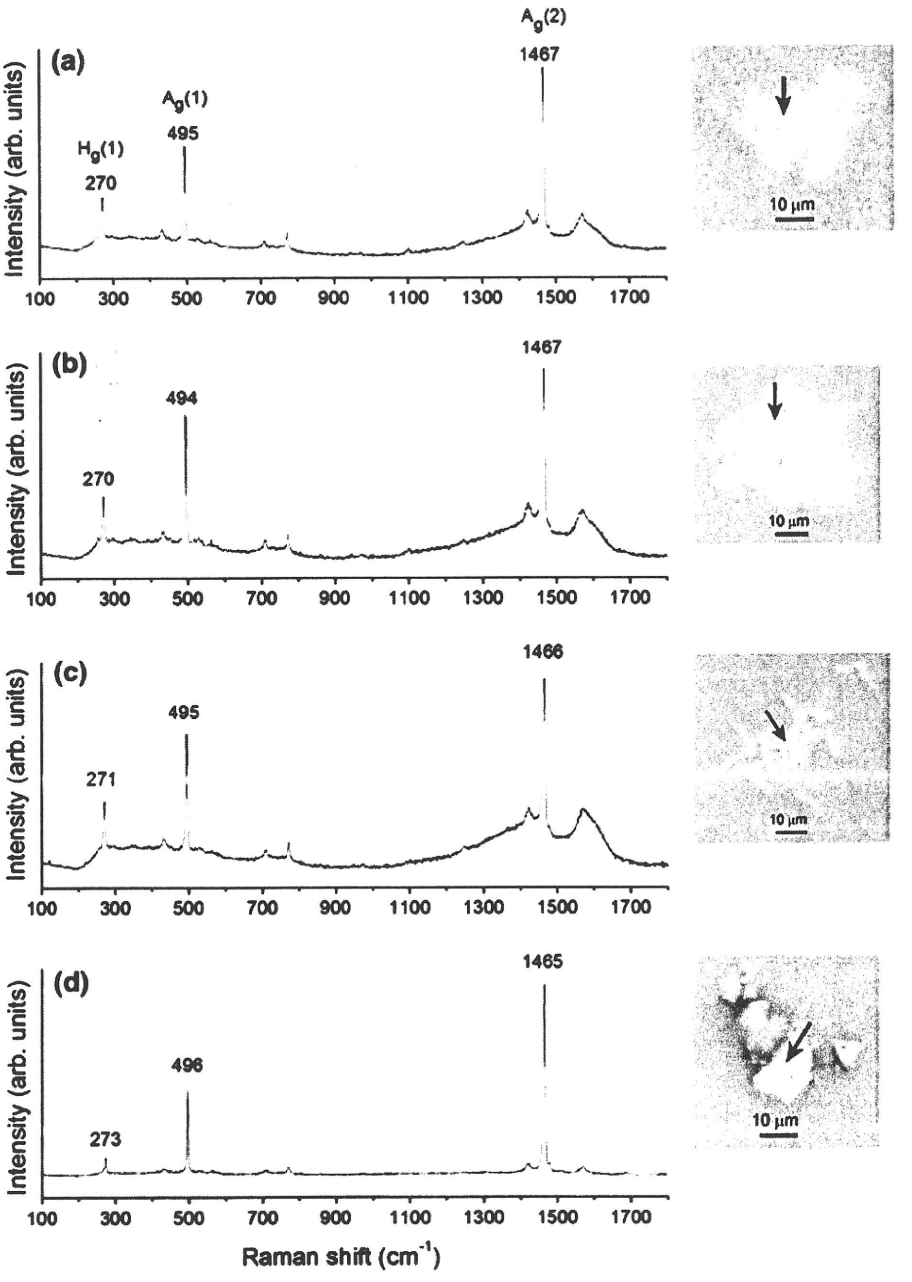

Fig. 5 Raman spectra of the C_{60} precipitates prepared by using IPA containing. **a** 0 mass% H_2O, **b** 1.3 mass% H_2O, **c** 2.5 mass% H_2O, and **d** 2.8 mass% H_2O, respectively. The optical micrographs in **a**, **b**, and **c** show the measured C_{60}NWs and the micrograph in **d** shows the measured granular C_{60} precipitate. The places where the Raman spectra were obtained are indicated by *arrows*

Figures 5 and 6 show the Raman profiles for the C_{60}NWs synthesized by using IPA with and without the water (H_2O, D_2O) addition. The Raman profiles were obtained for the C_{60} precipitates dried in air.

The Raman profiles of Fig. 5a–c were obtained for the C_{60}NWs shown in the optical micrographs, while the Raman profile (d) was measured for the arrowed granular C_{60} single-crystal precipitate. The three strong peaks ($H_g(1)$, $A_g(1)$, $A_g(2)$) have almost similar wavenumbers irrespective of the H_2O content in IPA, showing that the H_2O addition does not influence the crystallographic structure of C_{60}NWs. It is noticed that the base line of profile (d) is much flatter than the other base lines of (a), (b) and (c) Raman profiles. This result indicates that the single-crystal C_{60} precipitates have a better crystallinity than the C_{60}NWs.

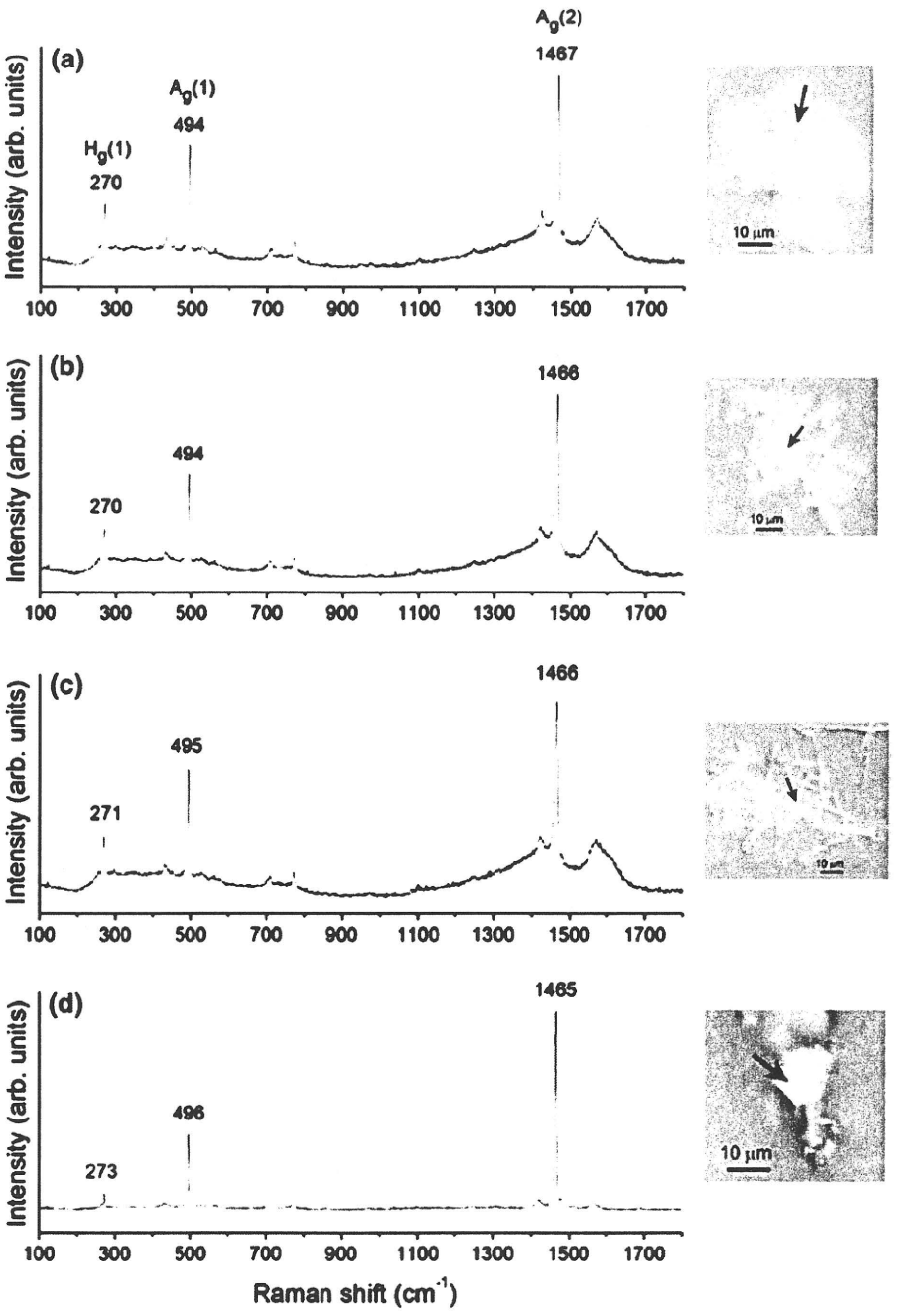

Fig. 6 Raman spectra of the C_{60} precipitates prepared by using IPA containing **a** 1.3 mass% D_2O, **b** 2.5 mass% D_2O, **c** 2.8 mass% D_2O, and **d** 3.8 mass% D_2O, respectively. The optical micrographs in **a**, **b**, and **c** show the measured C_{60}NWs and the micrograph in **d** shows the measured granular C_{60} precipitate. The places where the Raman spectra were obtained are indicated by *arrows*

The Raman spectroscopy measurement was also performed for the C_{60}NWs prepared by using IPA added with D_2O as shown in Fig. 6. Like the cases of Fig. 5, the $H_g(1)$, $A_g(1)$, and $A_g(2)$ peaks have similar wavenumbers, showing that the addition of D_2O does not influence the crystallographic structure of C_{60}NWs. The granular single-crystal C_{60} precipitate has the base line much flatter than those of C_{60}NWs like the case of Fig. 5, showing the better crystallinity than the C_{60}NWs.

Although both the H_2O and D_2O additions do not give clear influences on the crystallographic structure of C_{60}NWs, the addition of H_2O and D_2O was found to give the strong influence on the morphology of C_{60} precipitates and their stability in solution.

Preparation of short C_{60}NWs

As described in the introductory part, the growth control of C_{60}NWs is of importance for their application to organic thick film solar cells. Somani et al. fabricated short C_{60}NWs with lengths between 2 and 5 μm and diameters between 500 and 1000 nm by a modified LLIP method, where a C_{60}-saturated toluene solution was added to IPA drop by drop. Hence, this method does not form a stable liquid–liquid interface and instantaneously produces short C_{60}NWs. This method is very similar to our method that produces short C_{60}NWs by adding droplets of C_{60}-saturated toluene solution into IPA under ultrasonication (Miyazawa et al. 2005).

However, in the modified LLIP method of this paper, as shown in the experimental part, a stable liquid–liquid interface is first produced and then the interface is forcibly disturbed by manual mixing in order to obtain homogeneously precipitated C_{60}NWs. Using this method, very short C_{60}NWs with an average length of 1.8 ± 0.8 μm and an average diameter of 387 ± 131 nm were successfully synthesized as shown in the scanning electron microscopy (SEM) image of Fig. 7. The inset image shows a magnified image of the arrowed C_{60}NW with a hexagonal cross-section. The hexagonal cross-sectional image reflects the hexagonal crystal structure of C_{60}NWs grown in solution (Minato and Miyazawa 2005).

Figure 8 shows the distributions of length, diameter, and aspect ratio (length/diameter) of the above C_{60}NWs. The C_{60}NWs have lengths less than 5.5 μm,

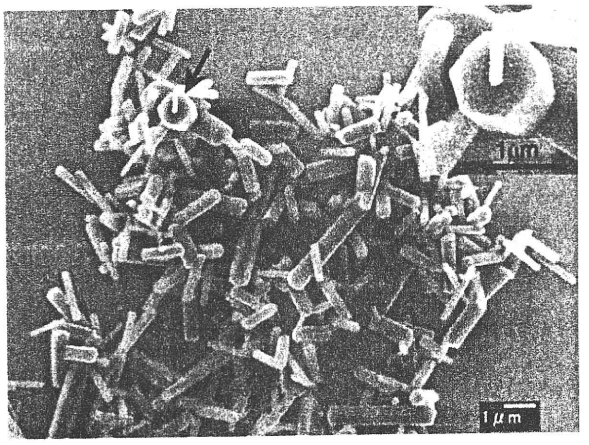

Fig. 7 SEM image of the short C_{60}NWs synthesized by a modified LLIP method. The *inset* shows a magnified image of the *arrowed* part

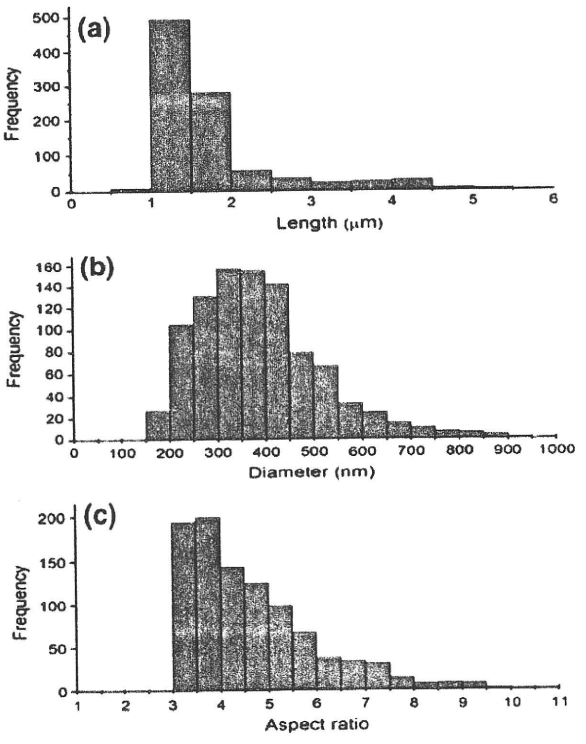

Fig. 8 **a** Length, **b** diameter, and **c** aspect ratio (length/diameter) distributions of the synthesized short C_{60}NWs

diameters less than 900 nm, and their aspect ratio ranges from 3 to 10. Since fibers are defined as particles with a length at least three times their diameter (The Royal Society and the Royal Academy of Engineering 2004), the synthesized short C_{60}NWs can be classified into the category of fibers with the smallest aspect ratio.

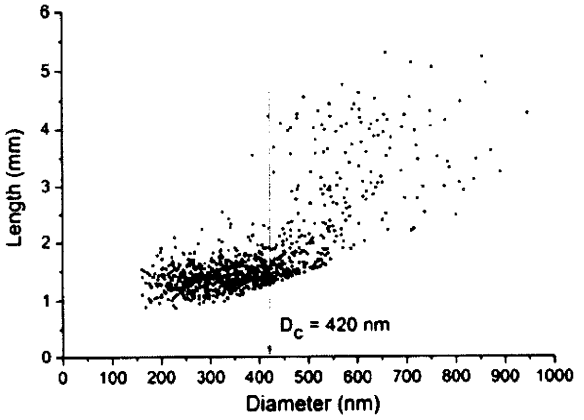

Fig. 9 Relationship between length and diameter of the C_{60}NWs synthesized at 15 °C using a C_{60}-saturated toluene solution and IPA at a volume ratio of 1:3

As shown above, the C_{60}NWs synthesized by us have the diameters and lengths smaller than those ever reported. The newly synthesized short C_{60}NWs would be more appropriate for the organic thick film solar cell application using C_{60}NWs. As shown in Fig. 9, it is observed that C_{60}NWs grow longer above the diameters greater than about 420 nm. This diameter (~420 nm) is regarded as a critical diameter D_c above which C_{60}NWs start to grow rapidly (Miyazawa and Hotta 2010). On the other hand, the D_c value for the growth temperature of 20 °C and the same solvent ratio of 1 (toluene):3 (IPA) with the case of Fig. 9, the D_c value was about 502 nm which is larger than the present value of 420 nm (Miyazawa and Hotta 2010). This fact is consistent with the hypothesis that the D_c value becomes smaller with increasing the supersaturation of C_{60} in solution with decreasing the growth temperature.

Conclusion

The above research can be summarized as follows.

(1) The stability of C_{60}NWs decreased and granular crystals of C_{60} appeared in the solutions prepared by using IPA added with excess amounts of water. The C_{60}NWs were found to be destabilized with time in the solutions added with water. These phenomena were observed in both of the experiments using H_2O and D_2O.

(2) The C_{60}NWs dried in air showed similar Raman profiles irrespective of the use of IPA with and without the water addition. The Raman profiles of granular C_{60} single crystals showed the base lines much flatter than those of C_{60}NWs, indicating that C_{60}NWs possess a disordered crystal structure.

(3) Short C_{60}NWs with aspect ratios ranging from 3 to 10 and an average length of about 1.8 μm were successfully fabricated. The short C_{60}NWs will be efficiently applied for the electrodes of organic thick film solar cells.

Acknowledgment Part of this research was supported by Health and Labour Sciences Research Grants (H21—Chemistry—Ippan-008) from the Ministry of Health, Labour and Welfare of Japan.

References

Guo JH, Luo Y, Augustsson A, Kashtanov S, Rubensson JE, Shuh DK, Ågren H, Nordgren J (2003) Molecular structure of alcohol–water mixtures. Phys Rev Lett 91:157401

Hotta K, Miyazawa K (2008) Growth rate measurement of C_{60} fullerene nanowhiskers. Nano 3:355–359

Hotta K, Miyazawa K (2009) Synthesis and growth investigation of C_{60} fullerene nanowhiskers. J Phys Conf Ser 159:012021

Kemp DD, Gordon MS (2008) An interpretation of the enhancement of the water dipole moment due to the presence of other water molecules. J Phys Chem A 112:4885–4894

Minato J, Miyazawa K (2005) Solvated structure of C_{60} nanowhiskers. Carbon 43:2837–2841

Minato J, Miyazawa K (2006) C_{60} fullerene tubes as removable templates. J Mater Res 21:529–534

Miyazawa K (2003) Creating nanofibers from fullerenes. NIMS NOW 1:2

Miyazawa K (2009) Synthesis and properties of fullerene nanowhiskers and fullerene nanotubes. J Nanosci Nanotechnol 9:41–50

Miyazawa K, Hotta K (2010) The effect of solvent ratio and water on the growth of C_{60} nanowhiskers. J Cryst Growth 312:2764–2770

Miyazawa K, Ringor C (2008) Platinum chloride deposition into C_{60} nanotubes. Mater Lett 62:410–413

Miyazawa K, Obayashi A, Kuwabara M (2001) C_{60} nanowhiskers in a mixture of lead zirconate titanate sol–C_{60} toluene solution. J Am Ceram Soc 84:3037–3039

Miyazawa K, Kuwasaki Y, Obayashi A, Kuwabara M (2002) C_{60} nanowhiskers formed by the liquid–liquid interfacial precipitation method. J Mater Res 17:83–88

Miyazawa K, Minato J, Mashino T, Yoshii T, Kizuka T, Kato R, Tachibana M, Suga T (2005) Characterization of the liquid-phase synthesized fullerene nanotubes and nanowhiskers. In: Proceedings of the second JSME/ASME international conference on materials and processing

2005—the 13th JSME materials and processing conference (M&P2005), Seattle, USA, 2005, p SMS-23

Nakao Y, Nagasawa H, Yamaoka R, Itoh H, Sakai Y, Tagashira H (1997) Influence of molecular structure on the propagation of streamer discharge in dielectric liquids. J Electrostat 40 and 41:199–204

Ogawa K, Kato T, Ikegami A, Tsuji H, Aoki N, Ochiai Y, Bird JP (2006) Electrical properties of field-effect transistors based on C_{60} nanowhiskers. Appl Phys Lett 88:112109

Ogawa K, Nobuyuki A, Miyazawa K, Nakamura S, Mashino T, Bird JP, Ochiai Y (2008) C_{60} nanowhisker field-effect-transistor application for nano-electronics. Jpn J Appl Phys 47:501–504

Sathish M, Miyazawa K, Sasaki T (2008) Preparation, characterization and electrochemical application of metal/metal-ion loaded fullerene nanowhiskers. J Solid State Electrochem 12:835–840

Somani PR, Somani SP, Umeno M (2007) Toward organic thick film solar cells: three dimensional bulk heterojunction organic thick film solar cell using fullerene single crystal nanorods. Appl Phys Lett 91:173503

Tachibana M, Kobayashi K, Uchida T, Kojima K, Tanimura M, Miyazawa K (2003) Photo-assisted growth and polymerization of C_{60} 'nano' whiskers. Chem Phys Lett 374: 279–285

The Royal Society and the Royal Academy of Engineering (2004) Nanoscience and nanotechnologies: opportunities and uncertainties. The Royal Society, London, p 37. http://www.nanotec.org.uk/report/chapter5.pdf

Wang Q, Zhang Y, Miyazawa K, Kato R, Hotta K, Wakahara T (2009) Improved fullerene nanofiber electrodes used in direct methanol fuel cells. J Phys Conf Ser 159:012023

Diamond & Related Materials 20 (2011) 299–303

Contents lists available at ScienceDirect

Diamond & Related Materials

journal homepage: www.elsevier.com/locate/diamond

Cross-sectional structural analysis of C_{60} nanowhiskers by transmission electron microscopy

Ryoei Kato, Kun'ichi Miyazawa *

Fullerene Engineering Group, Exploratory Nanotechnology Research Laboratory, National Institute for Materials Science, 1-1, Namiki, Tsukuba, Ibaraki 305-0044, Japan

ARTICLE INFO

Article history:
Received 9 September 2010
Received in revised form 17 November 2010
Accepted 9 January 2011
Available online xxxx

Keywords:
Fullerene nanowhiskers
C_{60} nanowhiskers
Fullerene
Liquid–liquid interfacial precipitation method (LLIP)
Cross-section

ABSTRACT

Cross-sectional observations of C_{60} nanowhiskers (C_{60}NWs) were successfully conducted using the focused ion beam (FIB) method. The C_{60}NWs were observed to possess the core-shell structures with porous cores and dense surface thin layers. The size and number of pores decreased from the center to the surface, showing that the densification of C_{60}NWs proceeds from the surface to the center upon drying. A cross-sectional high-resolution transmission electron microscopy (HRTEM) image of a C_{60}NW showed a disordered structure comprising the domains with sizes on the order of 10 nm. The most frequently observed cross-sections were hexagons, reflecting the solvated hexagonal crystal structures of as-grown C_{60}NWs. From the observation of various cross-sectional shapes of C_{60}NWs with different diameters and crystallographic surface analysis, it is suggested that C_{60}NWs grow longer above a critical diameter D_c with the development of low-energy crystal surfaces.

1. Introduction

It has been known that the needle-like crystals of C_{60}, "C_{60} whiskers," exhibit anomalous properties depending on their diameter. Firstly, the electrical resistivity of C_{60} whiskers rapidly decreases with decreasing diameter [1,2], and secondly, the Young's modulus of C_{60} whiskers increases with decreasing diameter [3]. Since these anomalous properties are considered to be caused by some structural inhomogeneity along the radial direction of the whiskers, detailed cross-sectional structural investigations are necessary.

Up to now, the cross-sectional observations of C_{60} whiskers have been performed by using thin sliced samples prepared using microtome [1,4]. Our former observations showed that C_{60} whiskers were composed of thin slabs with a thickness of about 10 nm [5], and a high density of (111) stacking faults were observed in a cross-section of a C_{60} whisker that was prepared with a microtome [4].

Although the cross-sections of C_{60} whiskers with a thickness greater than 1 μm showed clear {111} crystal surfaces in Fig. 4 [1] and Fig. 7 [4], the other crystal surfaces were not well characterized owing to their irregular surface morphologies.

The determination of cross-sectional shapes of C_{60} whiskers is important. For example, the geometrical moment of inertia used in the measurement of their Young's modulus by bending testing in a transmission electron microscope (TEM) depends on the cross-sectional shape of the C_{60} whiskers [3,6,7].

Although the microtome technique is often used in preparing cross-sectional samples using a suitable glue to embed the samples, shear stresses are inevitably imposed on the samples. The shear stress may introduce lattice defects such as stacking faults and dislocations. The high-density stacking faults observed in the above cross-sectional images of C_{60} whiskers may have been introduced by the sample preparation process with a microtome.

On the other hand, the focused ion beam (FIB) is a powerful tool to prepare thin-foil samples for TEM observation [8]. The FIB method makes it possible to obtain thin-foil samples with desired thicknesses at selected sample locations, although some artifacts like dislocations and amorphous surface layers may be introduced owing to the high-energy ion sources [9,10]. The present study has been performed as the first trial to observe the cross-sectional samples of C_{60} whiskers prepared by the FIB method. "C_{60} nanowhiskers (C_{60}NWs)," C_{60} whiskers with diameters smaller than 1 μm, have been investigated, since they exhibit higher Young's moduli and lower electrical resistivities than thicker C_{60} whiskers [1–3].

2. Experimental procedure

C_{60}NWs were fabricated by the liquid–liquid interfacial precipitation method (LLIP method) using good solvent solutions such as pyridine, benzene and toluene saturated with C_{60} (MTR Ltd. 99.5% pure) and isopropyl alcohol (IPA) as a poor solvent [11–13].

As shown in Fig. 1, the C_{60}NWs were placed on a thin layer of polyvinyl alcohol (PVA) deposited on a Si substrate. The second PVA layer was carefully deposited on the C_{60}NWs to be able to locate the sample position for thinning by a scanning electron microscope (SEM)

* Corresponding author. Tel./fax: +81 29 860 4667.
E-mail address: miyazawa.kunichi@nims.go.jp (K. Miyazawa).

0925-9635/$ – see front matter © 2011 Elsevier B.V. All rights reserved.
doi:10.1016/j.diamond.2011.01.016

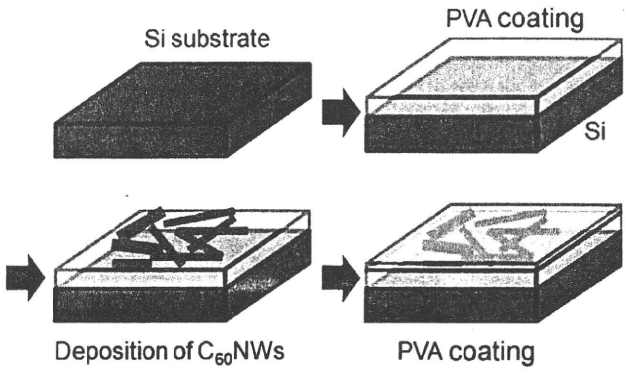

Fig. 1. The process used to prepare the sample with C_{60}NWs dispersed in a PVA film coated on a silicon substrate.

attached to an FIB system (Hitachi, FB-2100). Fig. 2 (a) and (b) show optical microscopy and SEM images of the embedded C_{60}NWs located at the same position on the sample. Since the second PVA layer was thin enough, traces of C_{60}NWs observed in the optical microscopy image could be recognized by the SEM of the FIB system and were easily subjected to the thinning process by the Ga ion source (15–40 keV, 0.01–2.8 nA) after depositing a protective tungsten (W) film. The cross-sectional morphology and structure of the C_{60} whiskers were observed by TEM (200 kV, JEOL JEM-2010).

3. Results and discussion

A typical cross-sectional TEM image for the sample thinned by FIB is shown in the TEM image of Fig. 3 (a). Fig. 3 (b) is a side view SEM image of Fig. 3 (a), showing a thin foil with an edge thickness of about 240 nm. The top part of the sample shows a tungsten layer that was used as a protective coating layer in the FIB process. Among the five cross-sectional images (A–E), images A, B and C show clear hexagonal shapes, reflecting the hexagonal crystal structure of as-grown solvated C_{60} whiskers [14]. The diameter of whisker C is about 1 μm. The whiskers A, B, D and E have diameters less than 1 μm and are normally called "C_{60} nanowhiskers" as described above [15]. Although whiskers A and B have similar diameters and contain tiny pores inside (Fig. 4 (a)), whisker B shows an exceptionally large pore near its center. The formation of such a large pore indicates inhomogeneous densification of the solvated matrix. A circumcircle defined for the cross-section A of Fig. 4 (a) is shown in Fig. 4 (b).

Fig. 5 (a) shows a histogram of pore diameters measured for the cross-section of whisker A of Fig. 4 (a). Regarding the pore as an ellipse, the pore diameter was calculated as the average value between the major axis and the minor axis. The average pore size was calculated to be 8.3 ± 2.3 nm. The maximum pore diameter was observed to be about 19 nm. Fig. 5 (b) shows that the pore diameter becomes smaller near to the whisker surface, although the pore diameter shows a large scatter between ~5 nm and ~20 nm. As shown in Fig. 5 (c), the distance between the pores and the whisker center O was measured and expressed as a histogram. Using this radial distribution of pore-to-center distances, the area number density of pores per square micrometer was plotted as a function of the radial distance (Fig. 5 (d)). It was observed that the area number density of pores ranged from about 1000–2500 μm^{-2} within a radius of 150 nm from the whisker center and rapidly decreased towards the surface. Hence, the C_{60}NW A was found to have a core-shell structure with a porous core and dense surface layer. Taking the maximum radius of the porous region to be about 240 nm, the thickness of the dense surface shell was calculated to be about 150 nm. In addition, it is clear that the densification of C_{60}NWs proceeds from the surface to the center by drying. The anomalous mechanical and electrical properties of C_{60} whiskers that depend on the whisker diameter must be caused by the existence of porous cores. In the synthesis of C_{60}NWs using a

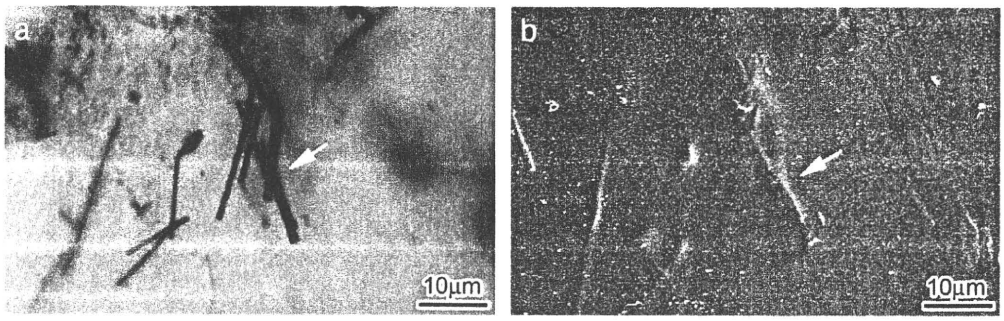

Fig. 2. (a) Optical microscopy image of the C_{60}NWs embedded in a PVA film and (b) SEM image of the area indicated by the arrow in (a). The C_{60}NWs were prepared by a C_{60}-saturated pyridine/IPA solution.

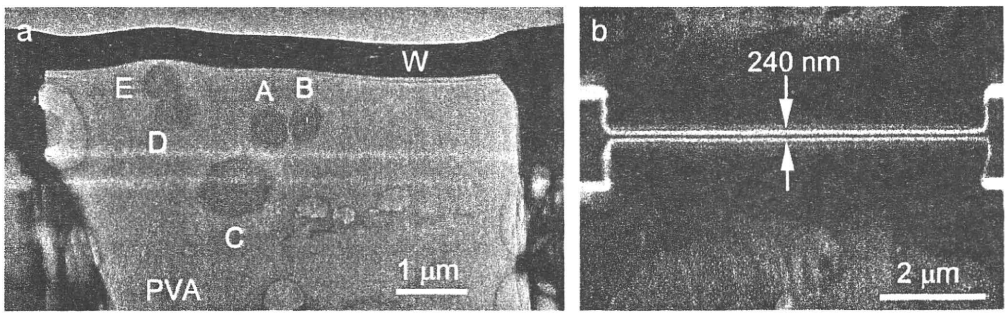

Fig. 3. (a) Cross-sectional TEM image of C_{60} whiskers embedded in a PVA film. The tungsten coating layer is shown by W. (b) Side-view SEM image for cross-section (a) with an edge thickness of 240 nm.

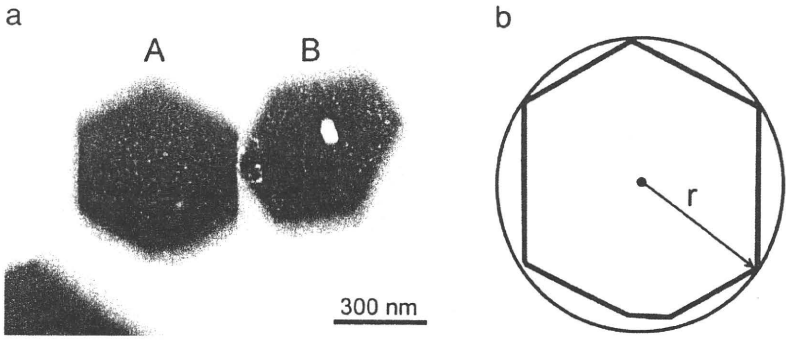

Fig. 4. (a) Magnified TEM image for cross-sections A and B of Fig. 3 (a). (b) Circumcircle defined for cross-section A with a diameter of 630 nm.

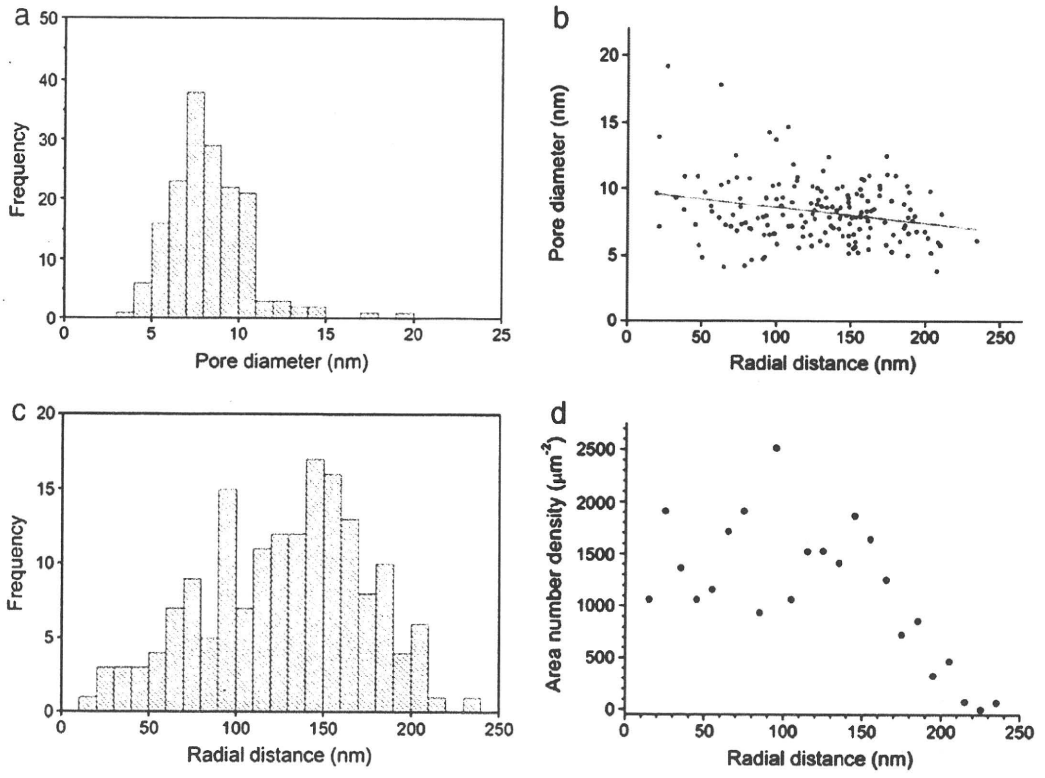

Fig. 5. (a) Pore diameter distribution of the C_{60}NW of Fig. 4 (a) A. (b) The pore diameter plotted as a function of the radial distance of pores measured from the circumcircle center (Fig. 4 (b)). (c) The radial distribution of pore number. (d) The area number density of pores plotted as a function of the radial distance of pores.

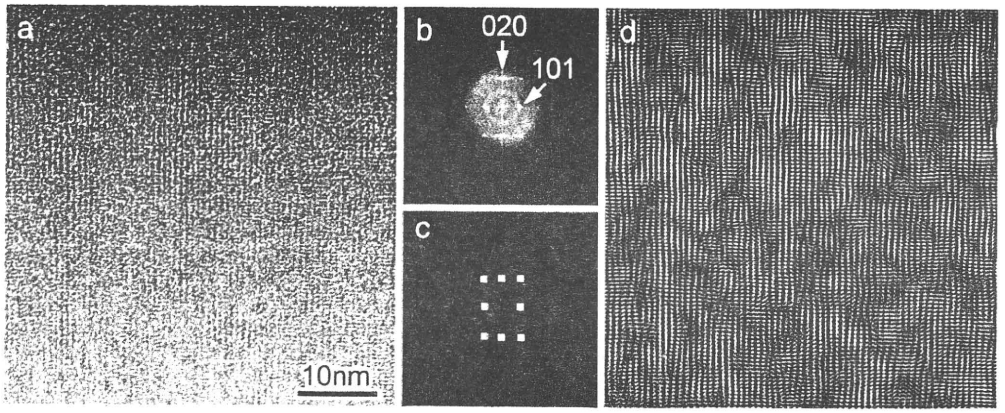

Fig. 6. (a) HRTEM image for the C_{60}NW of Fig. 4 (a) B viewed along [$\bar{1}$ 0 1] axis (bct). (b) FFT image for (a). (d) Inverse filtered FFT image for (a) constructed by using the filtered FFT pattern (c).

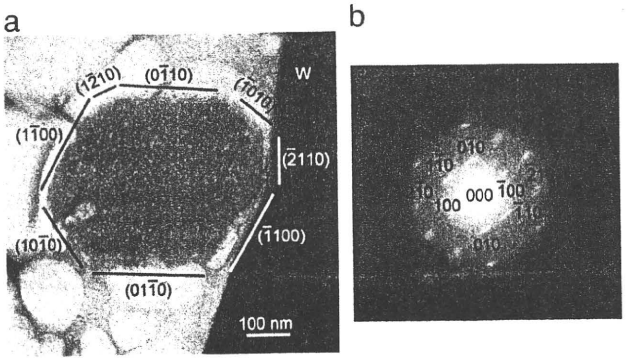

Fig. 7. (a) Cross-sectional TEM image of a C_{60}NW whose crystal faces are indexed by an hcp crystal system. (b) SAEDP for the TEM image (a) viewed along the [0 0 1] axis.

C_{60}-saturated toluene solution with the addition of a platinum derivative of C_{60}, $(\eta^2\text{-}C_{60})Pt(PPh_3)_2$, the C_{60}NWs were found to crystallize at the surface while the inner part showed a solvated soft structure [16]. This fact coincides with the present observation.

Although most of the solvent molecules may escape from the matrix upon densification at the surface, the other residual solvent molecules near the cores are conjectured to form tiny liquid bubbles and result in the formation of pores. In this study, the minimum pore size was observed to be 3.9 nm. This suggests that the critical pore diameter above which the pores can grow is about 4 nm.

Fig. 6 (a) is an HRTEM image of the cross-section shown in Fig. 4 (a) B. The fast Fourier transform (FFT) image (b) for (a) was indexed as shown in the figure, assuming a body-centered tetragonal (bct) structure with lattice constants $a = 0.99$ nm and $c = 1.5$ nm [1,3,11]. Fig. 6 (d) is an inverse FFT image formed by using the filtered FFT pattern of Fig. 6 (c). Fig. 6 (d) shows that the matrix of C_{60}NW is heavily disordered and exhibits domains with short-range ordering on the order of 5–10 nm. The intercluster distance between C_{60} molecules in the whisker is 0.99 nm. Since pristine C_{60} crystals have a face-centered cubic (fcc) structure with lattice constant $a = 1.4166$ nm [17] and the nearest neighbor distance of C_{60} molecules is 1.002 nm, the smaller intercluster distance of 0.99 nm suggests the formation of C_{60} polymer chains along the whisker growth axis. The polymerization of C_{60} molecules can occur by the irradiation of electron beams by TEM [18] which leads to the formation of bct structure from the pristine fcc structure.

Fig. 7 (a) shows a cross-sectional TEM image of a C_{60}NW with 8 vertices. The selected-area electron diffraction pattern (SAEDP) for Fig. 7 (a) is shown in Fig. 7 (b) and could be indexed by assuming a hexagonal close-packed (hcp) crystal system with lattice constant $a = 0.96$ nm. It has been known that pure C_{60} crystals can take both the hcp structure as well as the fcc structure [17,19–21]. In this example, the intercluster distance of C_{60} molecules equals 0.96 nm and is smaller than that of pristine C_{60}, suggesting electron beam polymerization. Although the length of the c-axis cannot be obtained from the SAEDP, it is calculated to be 1.6 nm by assuming a c/a ratio of 1.633 of the hcp structure [19–21]. This c-axis length is close to that of 1.5 nm of the bct system shown above.

The C_{60}NW is surrounded by the 8 crystal faces that were indexed by the Miller indices of the hexagonal system. It is found that the well-developed surfaces are the low-energy planes with low Miller indices such as $(10\bar{1}0)$, $(01\bar{1}0)$ and $(1\,\bar{1}\,0\,0)$. The smaller $(\bar{2}\,1\,1\,0)$ and $(1\,\bar{2}\,1\,0)$ crystal surfaces must have higher energy than the other crystal surfaces with lower Miller indices.

Fig. 8 (a) shows the number of vertices counted for the various observed cross-sections and expressed as a function of the diameter of C_{60}NWs. Although the number of whisker vertices ranges from 6 to 8, the most frequently observed cross-section is hexagonal as expected from the solvated hexagonal structures in solution [13,14]. No special relationship was found between the diameter and the number of vertices. However, as shown in the TEM images of B, C and D of Fig. 8 (b), the cross-section of C_{60}NWs prepared by the C_{60}-saturated benzene/IPA solution becomes irregular with decreasing diameter below 100 nm. The above result suggests that the low-energy crystal faces with low Miller indices develop with increasing whisker diameter above a critical diameter (D_c). The D_c value may be about 100 nm in the case of the benzene/IPA solvent system, since the cross-section A with a diameter of about 100 nm shows a hexagonal shape. In general, the C_{60}NWs are expected to start to grow longer when their diameter becomes greater than the critical diameters in order to develop the low-energy crystal surfaces [22]. The rounded cross-section D suggests the initial isotropic growth of C_{60}NWs.

4. Conclusions

The above research can be summarized as follows:

(1) Cross-sections of C_{60}NWs were successfully obtained through the FIB process by using samples embedded in PVA films.
(2) C_{60}NWs have a core-shell structure with dense surface thin layers and porous inner cores with mean pore diameters of about 8 nm. The number and size of the pores decrease near the surface of C_{60}NWs.
(3) The intercluster distance of the C_{60} molecules of C_{60}NWs was found to be smaller than that of pristine C_{60} crystals by TEM observations, indicating the polymerization of C_{60} molecules by electron beam irradiation.

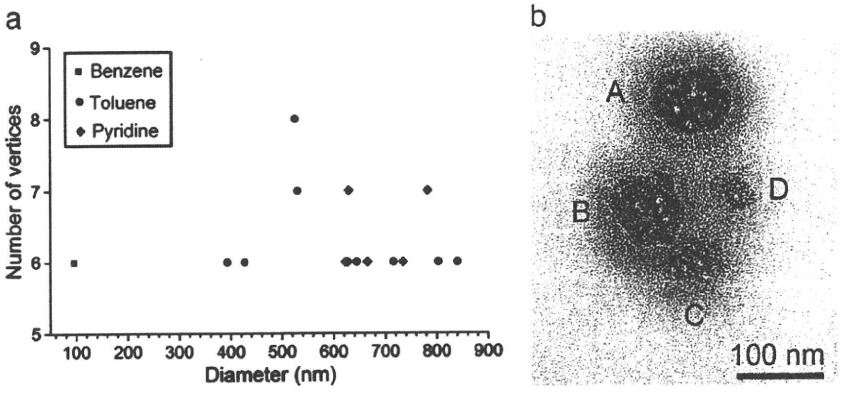

Fig. 8. (a) The number of vertices plotted as a function of diameter for the C_{60}NWs synthesized using C_{60}-saturated benzene/IPA, C_{60}-saturated toluene/IPA and C_{60}-saturated pyridine/IPA solutions. (b) Cross-sectional TEM image of the C_{60}NWs synthesized using C_{60}-saturated benzene/IPA solution.

(4) The FFT analysis for an HRTEM cross-sectional image of C_{60}NW revealed a disordered matrix composed of domains with sizes on the order of 5–10 nm.
(5) The most frequently observed cross-section of C_{60}NWs was hexagonal. A C_{60}NW was observed to be surrounded by crystal surfaces with low Miller indices of the hexagonal crystal system. It is suggested that C_{60}NWs grow longer above a critical diameter (D_c) by developing low-energy crystal surfaces.
(6) The cross-sections of C_{60}NWs became irregular and rounded with decreasing whisker diameter, suggesting the isotropic growth of C_{60}NWs with diameters smaller than D_c during their initial nucleation and growth stage.

Acknowledgements

Part of this research was supported by Health and Labour Sciences Research Grants (H21-Chemistry-Ippan-008) from the Ministry of Health, Labour and Welfare of Japan and conducted in Center for Nano Lithography & Analysis, The University of Tokyo, supported by the Ministry of Education, Culture, Sports, Science and Technology (MEXT), Japan. This work was also supported in part by World Premier International Research Center (WPI) Initiative on Materials Nanoarchitectonics, MEXT, Japan.

References

[1] K. Miyazawa, Y. Kuwasaki, K. Hamamoto, S. Nagata, A. Obayashi, M. Kuwabara, Surf. Interface Anal. 35 (2003) 117.
[2] M.P. Larsson, J. Kjelstrup-Hansen, S. Lucyszyn, ECS Trans. 2 (2007) 27.
[3] K. Saito, K. Miyazawa, T. Kizuka, Jpn. J. Appl. Phys. 48 (2009) 010217.
[4] K. Miyazawa, K. Hamamoto, S. Nagata, T. Suga, J. Mater. Res. 18 (2003) 1096.
[5] K. Miyazawa, A. Obayashi, M. Kuwabara, J. Am. Ceram. Soc. 84 (2001) 3037.
[6] T. Kizuka, K. Saito, K. Miyazawa, Diamond Relat. Mater. 17 (2008) 972.
[7] K. Asaka, R. Kato, K. Miyazawa, T. Kizuka, Appl. Phys. Lett. 89 (2006) 071912.
[8] B. Wei1, P. Kohler-Redlich, U. Bäder, B. Heiland, R. Spolenak, E. Arzt, M. Rühle, Ultramicroscopy 85 (2000) 93.
[9] K. Ogasawara, H. Kameda, Y. Matsuzaki, T. Sakurai, T. Uehara, A. Toji, N. Sakai, K. Yamaji, T. Horita, H. Yokokawa, J. Electrochem. Soc. 154 (2007) B657.
[10] M. Andrzejczuk, T. Płocińsski, W. Zieliński, K.J. Kurzydłowski, J. Microsc. 237 (2010) 439.
[11] K. Miyazawa, Y. Kuwasaki, A. Obayashi, M. Kuwabara, J. Mater. Res. 17 (2002) 83.
[12] K. Miyazawa, J. Minato, T. Yoshii, M. Fujino, T. Suga, J. Mater. Res. 20 (2005) 688.
[13] J. Minato, K. Miyazawa, Diamond Relat. Mater. 15 (2006) 1151.
[14] J. Minato, K. Miyazawa, Carbon 43 (2005) 2837.
[15] K. Miyazawa, J. Nanosci. Nanotechnol. 9 (2009) 41.
[16] K. Miyazawa, T. Suga, J. Mater. Res. 19 (2004) 2410.
[17] D. McCready, M. Alnajjar, Powder Diffraction File No. 44-558, International Centre for Diffraction Data, Newton Square, PA, (1994).
[18] M. Nakaya, T. Nakayama, M. Aono, Thin Solid Films 464–465 (2004) 327.
[19] W. Krätschmer, L.D. Lamb, K. Fostiropoulos, D.R. Huffman, Nature 347 (1990) 354.
[20] D.L. Dorset, J. Phys. Chem. 99 (1995) 16748.
[21] J.L. de Boer, S. van Smaalen, V. Petricek, M. Dusek, M.A. Verheijen, G. Meijer, Chem. Phys. Lett. 219 (1994) 469.
[22] K. Miyazawa, K. Hotta, J. Cryst. Growth 312 (2010) 2764.